JOURNAL OF SOLID STATE CHEMISTRY 112, 392–397 (1994)

On BSCCO Superconductor-Related $Bi_2Sr_2MnO_{6+x}$ and $BiPbSr_2MnO_6$: X-Ray Absorption Spectroscopy and Diffraction Study

M. Catti,* G. Dalba,† P. Fornasini,† and M. Mölgg*

*Dipartimento di Chimica Fisica ed Elettrochimica, Università di Milano, Via Golgi 19, 20133 Milano, Italy; and †Dipartimento di Fisica, Università di Trento, 38050 Povo (Trento), Italy

Received July 30, 1993; in revised form December 10, 1993; accepted December 14, 1993

$Bi_2Sr_2MnO_{6+x}$ and $BiPbSr_2MnO_6$, isotypic with the 2201 BSCCO superconductor, were investigated by X-ray powder diffraction and X-ray absorption spectroscopy (synchrotron radiation). The unit-cell constants are $a = 21.796(3)$, $b = 5.4268(7)$, $c = 23.612(2)$ Å, and $a = 5.3186(8)$, $b = 5.3892(8)$, $c = 23.765(3)$ Å, respectively. Superlattice modulation peaks ($h \neq 4n$) are evident in the diffractogram of the first phase. XAFS spectra at the K edge of manganese were recorded for the two compounds and for metallic Mn, MnO, and Mn_2O_3. An energy shift of about 1.5 eV is observed between the profiles of the two phases. By comparison of spectral features with those of the simple oxides, the oxidation state of Mn is inferred to be +2.6(1) and +2.9(1) in $Bi_2Sr_2MnO_{6+x}$ and $BiPbSr_2MnO_6$, respectively.

INTRODUCTION

Some interest has arisen recently for compounds obtained by full substitution of copper in the BSCCO family of oxidic superconductors (1, 2). Previous studies had concerned partial substitutions only, with the purpose of improving the superconductive performance, while a full replacement of Cu by another di- or trivalent transition metal usually leads to complete loss of superconductivity. Therefore, these investigations aim at a general understanding of the crystal-chemical features of Cu–O layers, which are thought to be connected to superconductive behavior, for instance, the Jahn–Teller distortion of coordination octahedra, and the magnetic behavior of the transition metal atom and its deviations from the +2 oxidation state related to vacant or interstitial sites of O atoms in the structure.

In the present work two Mn^{3+} analogues of the 2201 BSCCO phase are considered. These are interesting because Mn^{3+} shows a strong Jahn–Teller effect similarly to Cu^{2+}, while its different valence requires a charge compensation obtained either by changing the O contents or by a Bi^{3+}/Pb^{2+} substitution. The crystal structures of $Bi_2Sr_2MnO_{6+x}$ and $BiPbSr_2MnO_6$, refined by single-crystal X-ray diffraction, are reported in the literature (1, 3); that of the first compound was also studied by powder neutron diffraction (4), and the magnetic structure of its antiferromagnetic phase was determined as well (5). The structure of $Bi_2Sr_2MnO_{6+x}$ turns out to be commensurably modulated, owing to the presence of interstitial O atoms which balance the excess charge of Mn with respect to +2. However, the amount of oxygen was not measured directly, but rather inferred from the structure refinements: 6.5 and 6.38 atoms per formula unit, corresponding to +3 and +2.75 formal charges on Mn, were obtained in the neutron and X-ray cases, respectively.

It has thus seemed interesting to reconsider the problem of the Mn valence in these compounds by a different technique, that of X-ray absorption spectroscopy. It is well known that X-ray absorption edges undergo a chemical shift toward higher energies, in the passage from pure metal to its oxide. This is related to the tighter binding of the core level due to the reduction of screening effects and to the appearance of an energy gap between occupied valence and empty conduction states (6). The position and shape of the absorption edge of a transition metal in a compound are affected by physicochemical factors like oxidation state, coordination number, and the covalent character of the bonding (7). In the case of manganese oxides, where octahedral coordination is always observed, the chemical shift can be directly correlated to the oxidation state of the metal (8). This method was recently applied to the study of Mn impurities in YBCO, finding a +2 oxidation state by comparison with the spectra of MnO, Mn_3O_4, and Mn_2O_3 (9).

The X-ray powder diffraction patterns of both compounds were reinvestigated, with a particular aim at the detection of superlattice Bragg peaks in the lead-free phase.

SYNTHESIS AND X-RAY DIFFRACTION

The starting reagents used were Bi_2O_3, PbO, SrO, and Mn_2O_3. The first two oxides were analytical-grade commercial products, while the other two were prepared by

0022-4596/94 $6.00

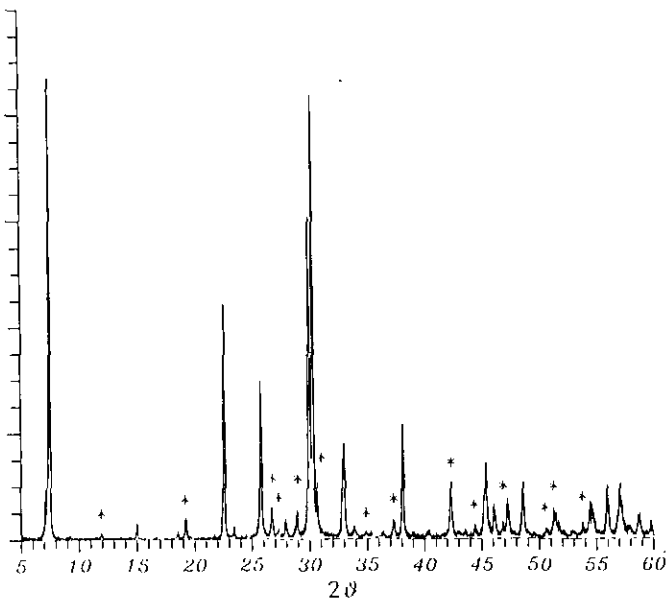

FIG. 1. X-ray powder diffraction pattern of $Bi_2Sr_2MnO_{6+x}$ (Cu$K\alpha$ radiation). Superlattice Bragg peaks ($h \neq 4n$) are marked by asterisks.

thermal decomposition of $SrCO_3$ at 1050°C under vacuum and of $Mn(CH_3COO)_3 \cdot 2H_2O$ or MnO_2 at 750°C in air, respectively. SrO and Mn_2O_3 were chosen, rather than $SrCO_3$ and MnO_2 as in the previous reported preparation (1), to avoid the evolution of gaseous CO_2 during the reactions and to better control the wanted oxidation state +3 of Mn in the final compounds. A flowing Ar atmosphere was used to prevent oxidation of Mn^{+3} to Mn^{+4} in all annealings described below.

The lead-free compound was obtained by subsequent heat treatments of 15 hr at 800, 900, and 950°C of a stoichiometric sample of mixed oxides ground and pelletized each time. Powder X-ray diffraction showed the presence of a single phase isostructural with BSCCO 2201. A slightly different synthesis route, involving the preparation of $Sr_2Bi_2O_5$ by solid state reaction of Bi_2O_3 and $SrCO_3$ at 800°C in air, and then the reaction $Sr_2Bi_2O_5 + \frac{1}{2}Mn_2O_3 \rightarrow Bi_2Sr_2MnO_{6+x}$, gave similar results. All attempts to perform the synthesis in air led to formation of the $SrMnO_3$ perovskite plus $SrBi_2O_4$, while by vacuum operation Mn_2O_3 and Bi_2O_3 were reduced to MnO and to metallic Bi, respectively.

$BiPbSr_2MnO_6$ was prepared by reaction of the simple oxides at 800°C (15 hr), followed by a further heat treatment at 900°C (20 hr) with intermediate regrinding and pelletizing. No presence of other unwanted phases was detected by X rays. Alternatively, the reaction $PbO + \frac{1}{2}Bi_2O_3 + SrO + SrMnO_{2.5} \rightarrow BiPbSr_2MnO_6$ at 800°C (20 hr) also yielded a pure compound at lower temperature.

The intermediate phase $SrMnO_{2.5}$ was obtained by the reaction $SrCO_3 + \frac{1}{2}Mn_2O_3 \rightarrow SrMnO_3$ at 1000°C in air (24 hr), and by decomposition of $SrMnO_3$ at 1100°C in high vacuum (6×10^{-5} mbar, 48 hr).

The prepared compounds were studied by powder X-ray diffractometry (Siemens D500 apparatus, Cu$K\alpha$ radiation with diffracted beam monochromator. Measurement conditions: t(step) = 5 sec, $\Delta(2\Theta) = 0.01°$, $2\Theta_{max} = 85°$). The powder pattern of $Bi_2Sr_2MnO_{6+x}$ (Fig. 1) could be indexed on the basis of the supercell $a = 4 \times a_0$, b, c related to the orthorhombic, pseudo-tetragonal a_0, b, c cell of 2201 BSCCO (3). In the list of d_{hkl} values with relative intensities (Table 1), the superlattice Bragg peaks are those with $h \neq 4n$, and they are marked by asterisks in Fig. 1: they should not be misinterpreted as being due to impurity phases in the sample. Results for the Pb compound, where no structural modulation is present, are reported in Table 2 and Fig. 2. The unit-cell constants of both compounds were least-squared refined on the basis of measured d_{hkl} values, yielding the following results: a = 21.796(3), b = 5.4268(7), c = 23.612(2) Å ($Bi_2Sr_2MnO_{6+x}$), and a = 5.3186(8), b = 5.3892(8), c = 23.765(3) Å ($BiPbSr_2MnO_6$). The values obtained for the lead-free phase compare well with those from single-crystal X-ray data (1), but differ significantly (a, b shorter and c longer) from powder neutron results (4). This could indicate that the oxygen contents in our sample is lower than 6.5, according to Ref. (4). As for the Pb compound, the present results show a and b shorter and c longer (by about 0.01 Å) with respect to previous data (1).

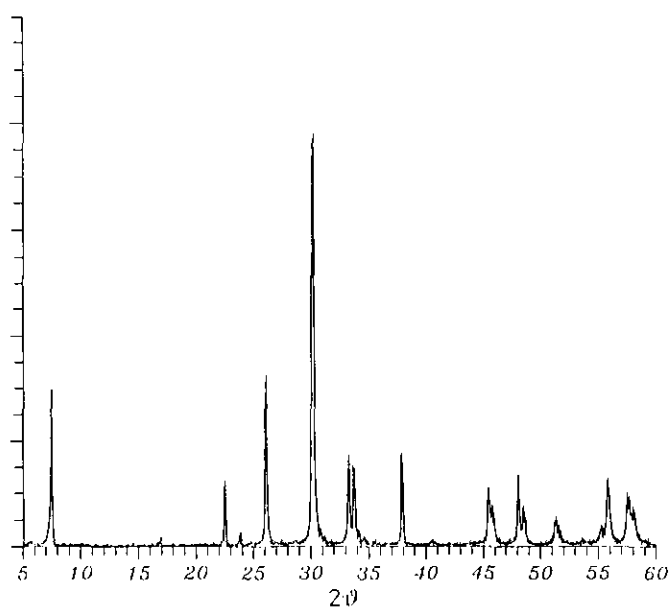

FIG. 2. X-ray powder diffraction pattern of $BiPbSr_2MnO_6$ (Cu$K\alpha$ radiation).

TABLE 1
Observed and Calculated d_{hkl} Values (Å), and Relative Observed Intensities, for the X-Ray Powder Pattern of $Bi_2Sr_2MnO_{6+x}$

h	k	l	d_{obs}	d_{calc}	I_{obs}
0	0	2	11.754	11.806	100
1	0	3	7.409	7.403	1
0	0	4	5.890	5.903	3
1	0	5	4.612	4.615	5
0	0	6	3.930	3.935	51
4	1	1	3.791	3.795	3
4	1	3	3.451	3.455	34
1	0	7	3.334	3.333	7
5	1	2	3.266	3.266	2
7	0	1	3.088	3.087	6
4	1	5	2.980	2.982	70
0	0	8	2.949	2.951	96
3	1	6	2.917	2.918	11
8	0	0	2.722	2.725	17
0	2	0	2.713	2.713	21
0	2	2	2.642	2.644	2
2	2	2	2.569	2.570	2
4	1	7	2.537	2.536	1
9	0	1	2.408	2.409	4
0	0	10	2.360	2.361	25
0	2	6	2.235	2.234	1
3	2	6	2.135	2.135	12
7	2	1	2.038	2.038	3
8	0	8	2.001	2.002	12
0	2	8	1.998	1.998	14
0	0	12	1.968	1.968	7
2	0	12	1.937	1.936	2
8	2	0	1.923	1.923	8
4	1	11	1.874	1.874	12
9	2	1	1.802	1.802	2
8	0	10	1.785	1.784	3
0	2	10	1.781	1.781	6
2	3	1	1.779	1.779	5
5	1	12	1.702	1.703	3
12	1	3	1.683	1.683	6
4	3	3	1.678	1.677	6
4	1	13	1.642	1.642	11
4	3	5	1.613	1.613	12
8	1	11	1.610	1.610	9
0	2	12	1.593	1.593	3
12	0	8	1.546	1.547	3
4	1	14	1.544	1.545	3
0	3	9	1.490	1.489	2
8	3	3	1.481	1.480	2
0	0	16	1.476	1.476	4
0	2	14	1.433	1.432	2
5	0	16	1.398	1.398	2
0	4	0	1.356	1.357	3
16	0	2	1.354	1.353	4
12	1	11	1.344	1.343	2
4	3	11	1.340	1.341	2
0	2	16	1.296	1.296	2
8	2	14	1.268	1.268	2
12	3	3	1.266	1.265	1
4	3	13	1.247	1.248	3
4	1	18	1.241	1.242	3
12	3	5	1.238	1.237	2
8	4	0	1.215	1.214	2
4	1	19	1.183	1.182	3
8	2	16	1.171	1.171	2
16	1	10	1.153	1.153	2
4	4	10	1.149	1.150	2

Note. Reflections with $h \neq 4n$ (n is any integer) are the superlattice Bragg peaks.

X-RAY ABSORPTION SPECTROSCOPY

Experimental

XAFS (X-ray absorption fine structure) measurements were carried out on the two Mn analogues of 2201 BSCCO phases and, for comparison, on metallic Mn foil and on the MnO and Mn_2O_3 oxides. MnO and Mn_2O_3 were prepared by thermal decompositions of $MnCO_3$ in vacuum

TABLE 2
Observed and Calculated d_{hkl} Values (Å), and Relative Observed Intensities, for the X-Ray Powder Pattern of $BiPbSr_2MnO_6$

h	k	l	d_{obs}	d_{calc}	I_{obs}
0	0	2	11.817	11.883	10
0	1	1	5.250	5.256	2
0	0	6	3.956	3.961	15
1	1	1	3.737	3.739	3
1	1	3	3.414	3.416	40
1	1	5	2.962	2.961	100
0	2	0	2.693	2.695	21
2	0	0	2.659	2.660	19
0	2	2	2.627	2.628	3
2	0	2	2.596	2.596	2
1	1	7	2.529	2.528	1
0	0	10	2.375	2.377	23
0	2	6	2.229	2.228	1
2	0	6	2.208	2.208	1
0	2	8	1.996	1.996	14
2	0	8	1.981	1.982	10
2	2	0	1.894	1.893	15
1	1	11	1.877	1.877	9
0	2	10	1.783	1.782	6
2	0	10	1.772	1.772	4
1	3	3	1.664	1.664	5
3	1	3	1.647	1.648	14
1	1	13	1.646	1.646	11
1	3	5	1.602	1.602	11
2	2	8	1.598	1.596	11
2	0	12	1.590	1.589	6
0	0	16	1.486	1.485	6
2	2	10	1.481	1.481	6

at 800°C and of MnO_2 in air at 750°C, respectively, and their powder diffraction patterns were in good agreement with the JCPDS-ICDD standards both before and after XAFS measurements. All samples were finely powdered and deposited on filter membranes by a sonication technique, in order to obtain homogeneous specimens of controlled thickness. The surface density was 4 to 6 mg cm^{-2} in all cases; the corresponding jumps at the Mn K edge were $\Delta(\mu z) = 1, 2$, and 0.2 for MnO, Mn_2O_3, and the two BSCCO-type oxides, respectively (μ is the absorption coefficient and z is the thickness). Test measurements done after doubling the sample thickness did not reveal any detectable thickness effect.

The experiments were performed at the PWA-BX2 wiggler beam line of the Adone Synchrotron Light Source in Frascati (Italy). The electron energy, maximum stored current, and wiggler magnetic field were 1.5 GeV, 60 mA, and 1.6 T, respectively. A channel-cut silicon crystal with (111) parallel reflecting faces was used as a monochromator, and the photon flux was measured by argon-filled ionization chambers. The overall energy resolution at the Mn K edge (6539 eV) was estimated to be 1.5 eV, taking into account the comparable contributions of the angular divergence of the beam, the monochromator rocking curve, and the core-level width. Data were recorded with 0.5-eV steps, and the energy position was controlled by an absolute angular encoder. Repeated measurements on the same sample differed by less than 0.1 eV in the energy position of fine structures and no more than 1% in amplitude.

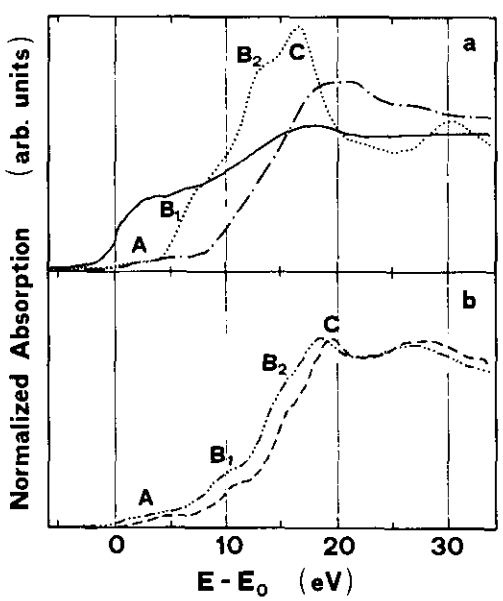

FIG. 3. X-ray absorption spectra at the K edge of manganese for: (a) metallic Mn (solid line), MnO (dotted line), and Mn_2O_3 (dash-dotted line), and (b) $Bi_2Sr_2MnO_{6+x}$ (dash-dotted line) and $BiPbSr_2MnO_6$ (dashed line). The energy scale is relative to the edge position of Mn (maximum of first derivative).

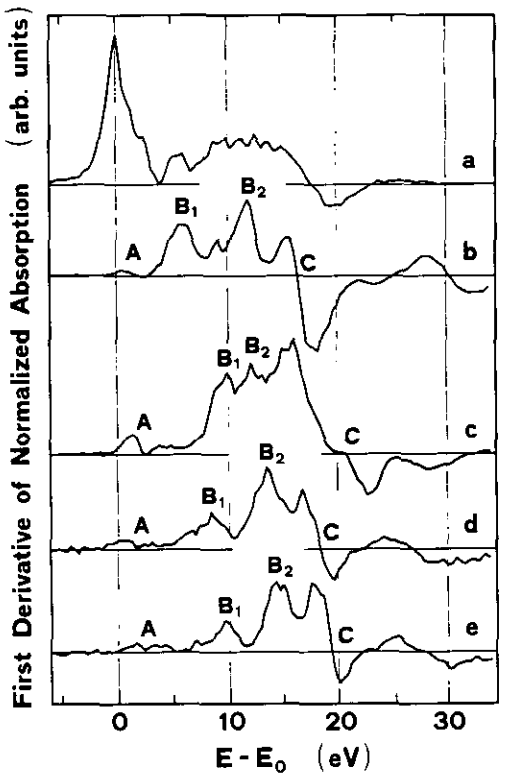

FIG. 4. First derivatives of X-ray absorption spectra of Mn (a), MnO (b), Mn_2O_3 (c), $Bi_2Sr_2MnO_{6+x}$ (d), and $BiPbSr_2MnO_6$ (e).

Results and Discussion

The contribution of the K edge of manganese to the overall X-ray absorption coefficient was isolated by subtracting from the spectra a Victoreen-like curve best fitting the preedge smooth behavior. The resulting spectra of Mn, MnO, and Mn_2O_3 and those of the two BSCCO-like compounds are shown in Figs. 3a and 3b, respectively. In Fig. 4 the corresponding first-derivative curves appear. The energy scales have zeros at the main edge jump of metallic manganese, taken in correspondence with the maximum of the first derivative. The amplitudes of all spectra (Fig. 3) were normalized in the high-energy region (above 30 eV).

Let us first examine the spectra of metallic Mn and its simple oxides. The edge of Mn is characterized by a shoulder, corresponding to the maximum of the first derivative, and by a main peak at about 17 eV. Both features can be ascribed to dipole-allowed transitions from the 1s core level to empty states of p symmetry at the bottom of the conduction band. The edges of the oxides show two shoulders B1 and B2 and a main peak C, whose positions are determined by the corresponding

TABLE 3

Positions of the Main Features of the X-Ray Absorption Spectra of Mn Oxides and Mn Analogues of 2201 BSCCO Superconductors

	MnO	Mn_2O_3	$Bi_2Sr_2MnO_{6+x}$	$BiPbSr_2MnO_6$
Onset of 3*d* pip (A)	0.7	1.2	0.2	1.7
First shoulder (B1)	6.2	10.2	8.7	9.7
Second shoulder (B2)	11.7	11.7	13.7	14.4
Main peak (C)	16.0	18.5–21.0	18.5	19.4

Note. The energy values (eV) are relative to the edge jump of metallic Mn.

local maxima and zero point of the derivative curves, respectively (Table 3). Overall edge shifts with respect to that of pure Mn are observed for both oxides. The relative shift between the two oxides is roughly constant along all the rising edge, in agreement with previous measurements (8). A quantitative assessment of the chemical shift can be based on the position of the B1 feature (Fig. 4), which corresponds to the onset of empty 4*p* states at the bottom of the conduction band (6 eV for MnO and 10 eV for Mn_2O_3). The differences of energy shifts between Mn_2O_3 and MnO are smaller for the second shoulder B2 and the main peak C than those for the first shoulder B1 (see also Table 3). However, it can be noted that the main peak C in Mn_2O_3 is quite flat and extends from 18.5 to 21 eV. As the metal atom shows a coordination number of 6 in both oxides, the relative shift of the B1 structure between MnO and Mn_2O_3 can be mainly ascribed to change of oxidation state from +2 to +3. Minor effects, particularly in the edge shapes, should be related to distortions of the coordination octahedra (e.g., the Jahn–Teller effect) and to influence of the outer coordination shells.

The spectra of the two Mn oxides also show a weak preedge feature (A) below 5 eV, which is typical of transition metal oxides and is generally ascribed (in centrosymmetric systems) to electric quadrupole transitions to states of *d* symmetry. These are generally considered to be bound states generated by the lack of screening of the core hole, or "core hole excitons" (10). However, in noncentrosymmetric systems this "3*d* pip" can also contain contributions from dipole transitions to hybridized *p*–*d* states; its strength can then be used to measure the deformation of the octahedron (7, 11, 12). In our case the strength is comparable in both oxides, which are centrosymmetric. The chemical shift of the 3*d* pip is weaker than that of the main edge (Table 3).

It should be remarked that the spectrum obtained for Mn_2O_3 differs substantially from that reported in Ref. (13), while it is similar to other previous results (8, 14). A possible reason is that a partial oxidation occurred in the sample used in the referred study (13), owing to the resemblence of its spectrum to that of MnO_2.

The two BSCCO-like phases show spectra with very similar shapes, though all features of the Pb-containing compound are shifted by 1.0–1.5 eV toward higher energies. Two shoulders B1 and B2 and a main peak C are observed, like in pure Mn oxides (Figs. 3b and 4); the preedge 3*d* pip A is present, too, with an intensity comparable to that of the oxides, consistently with an Mn coordination environment of octahedral type. On the other hand, by comparison of their overall edge positions with those of MnO and Mn_2O_3 (cf. also Table 3) both BSCCO-like compounds appear closer to the latter than to the former oxide.

However, clear evidence of slightly different effective charges on Mn in the two compounds is given by the small but significant energy shift between their spectra, while their very similar shapes should indicate equal geometrical environments of the metal atom. By the direction of the energy shift, we can infer that the oxidation number of Mn in the lead-free compound is slightly lower than that of the other one (which is close to +3, as expected from full charge balance by the Bi^{3+}/Pb^{2+} and Cu^{2+}/Mn^{3+} substitutions with respect to 2201 BSCCO). A linear relationship between effective charge and edge position is reported in the literature for various Mn compounds (13, 15). Further, recently the oxidation state of Mn in photosynthetic substances was evaluated by comparing their edge spectra with linear combinations of Mn^{2+}, Mn^{3+}, and Mn^{4+} spectra (16). A similar procedure was also utilized for copper in the YBCO superconductor (17). The valence of Mn in the two present compounds is estimated by a linear interpolation of the energy positions of the first shoulder B1 (Table 3) between the values of simple oxides MnO and Mn_2O_3. The result of this calculation gives oxidation states of 2.6 ± 0.1 and 2.9 ± 0.1 for Mn in $Bi_2Sr_2MnO_{6+x}$ and $BiPbSr_2MnO_6$, respectively. It follows that the value of x defining the oxygen contents per formula unit in the lead-free compound amounts to 0.3, and thus agrees better with the findings of the single-crystal X ray (3) than with those of the powder neutron (4) structure refinement.

CONCLUSIONS

X-ray diffraction and absorption spectroscopy are complementary techniques able to clarify the Mn^{3+}/Cu^{2+} aliovalent substitution in the 2201 BSCCO structure. In the $BiPbSr_2MnO_6$ case, Mn is very close to formal Mn^{3+}, and O is fully stoichiometric. This is shown by the XAFS spectrum, with its edge features corresponding roughly in energy to those of Mn_2O_3; extra oxygen atoms in interstitial positions in the structure should be excluded, and no modulation peaks appear in the diffraction pattern. On

the other hand, $Bi_2Sr_2MnO_{6+x}$ shows superlattice modulation peaks, and excess interstitial O atoms are present. The shift of its X-ray absorption spectrum toward lower energy indicates an oxidation state lower than +3, and the x value can be estimated to be around 0.3.

ACKNOWLEDGMENTS

Financial support from C.N.R. (Consiglio Nazionale delle Ricerche), Roma, is gratefully acknowledged. E. Burattini and F. Rocca and the technical staff of the Frascati PWA Laboratory are thanked for help in the XAFS measurements.

REFERENCES

1. J. M. Tarascon, Y. LePage, W. R. McKinnon, R. Ramesh, M. Eibschutz, E. Tselepis, E. Wang, and G. W. Hull, *Physica C* **167,** 20 (1990).
2. Y. LePage, W. R. McKinnon, J. M. Tarascon, and P. Barboux, *Phys. Rev. B* **40,** 6810 (1989).
3. J. M. Tarascon, Y. LePage, and W. R. McKinnon *Eur. J. Solid State Chem.* **27,** 81 (1990).
4. Z. Jirák, E. Pollert, D. Sedmidubský, M. Dlouhá, and S. Vratislav, *Physica C* **196,** 68 (1992).
5. W. R. McKinnon, E. Tselepis, Y. LePage, S. P. McAlister, G. Pleizier, J. M. Tarascon, P. F. Miceli, R. Ramesh, G. W. Hull, J. V. Waszczak, J. J. Rhyne, and D. A. Neumann, *Phys. Rev. B* **41,** 4489 (1990).
6. B. K. Agarwal, "X-Ray Spectroscopy." Springer-Verlag, Berlin, 1991.
7. J. Petiau, G. Calas, P. Bondot, C. Lapeyre, P. Levitz, and G. Loupias, *in* "EXAFS for Inorganic Systems" (C. D. Garner and S. S. Hasnain, Eds.). Daresbury Laboratory, SERC DL/SCI/R17, 1981.
8. E. E. Vainshtein, R. M. Ovrutskaya, B. I. Kotlyar, and V. R. Linde, *Sov. Phys. Solid State* **5,** 2150 (1964).
9. B. D. Padalia, S. J. Gurman, P. K. Mehta, and O. Prakash, *J. Phys. Condens. Matter* **4,** 8519 (1992).
10. A. Bianconi, *in* "X-Ray Absorption" (D. C. Koningsberger and R. Prins, Eds.). Wiley, New York, 1988.
11. G. Bunker, E. A. Stern, R. E. Blankenship, and W. W. Parson, *Biophys. J.* **37,** 539 (1982).
12. C. Y. Yang, S. M. Heald, J. M. Tranquada, Y. Xu, Y. L. Wang, A. R. Moodenbaugh, D. O. Welch, and M. Suenaga, *Phys. Rev. B* **39,** 6681 (1989).
13. M. Belli, A. Scafati, A. Bianconi, S. Mobilio, L. Palladino, A. Reale, and E. Burattini, *Solid State Commun.* **35,** 355 (1980).
14. G. Sankar, P. R. Sarode, and C. N. R. Rao, *Chem. Phys.* **76,** 435 (1983).
15. A. Qi-wu and J. Wong, *in* "EXAFS and Near Edge Structure III" (K. O. Hodgson, B. Hedmann, and J. E. Penner-Hahn, Eds.). Springer-Verlag, Berlin, 1984.
16. V. K. Yachandra, V. J. DeRose, M. J. Latimer, I. Mukerji, K. Sauer, and M. P. Klein, *Jpn. J. Appl. Phys.* **32**(Suppl. 2), 523 (1993).
17. B. Lengeler, M. Wilhem, B. Jobst, W. Schwaen, B. Seebacher, and U. Hillebrecht, *Solid State Commun.* **65,** 1545 (1988).